Modelling of silicon surfaces: a comparative study

1990 J. Phys.: Condens. Matter 2 10259

(http://iopscience.iop.org/0953-8984/2/51/004)

J. Phys.: Condens. Matter **2** (1990) 10259–10288. Printed in the UK

Modelling of silicon surfaces: a comparative study

J H Wilson, J D Todd and A P Sutton
Department of Materials, Oxford University, Parks Road, Oxford OX1 3PH, UK

Received 4 April 1990, in final form 5 September 1990

Abstract. A theoretical study of the Si(110)–1 × 1, Si(100)–2 × 1, Si(111)–2 × 1 and Si(113)–1 × 1 surfaces is presented. We use both the semi-empirical tight-binding bond model and the classical potential of Stillinger and Weber to describe interatomic forces. Energy minimization calculations are carried out in order to deduce the stable atomic configurations. We show that the semi-empirical tight-binding approach can produce results in reasonable agreement with other experimental and theoretical work and we demonstrate that charge transfer is not an important factor governing the stability of these surfaces. In a comparative study, involving not only static energy minimization but also Monte Carlo simulated annealing, we show why the classical potential does not perform well in describing surface atomic structure.

1. Introduction

Scanning tunnelling microscopy (STM) [1] has enabled many details of surface atomic and electronic structure to be characterized directly in real space. The experimental information which has become available through STM provides a powerful challenge to theory to explain why surfaces adopt particular atomic configurations. Semiconductor surfaces are especially interesting, not only because of their importance in the development of novel electronic devices, but also from a fundamental point of view because of the wide variety of unexpected reconstructions that can occur. We are therefore motivated to model the atomic structure of a number of silicon surfaces.

Broadly there are three main approaches which can be adopted. These are *ab initio* local density functional calculations [2], semi-empirical calculations in which a formal expression for the energy derived from first principles is parameterized [3–8] and empirical calculations in which an interaction potential which may contain any number of N-body terms is empirically fitted to describe one region of configuration space in the hope that it will also be able to model other regions successfully [9]. A large number of empirical potentials for silicon has been proposed in recent years [10–16]. The *ab initio* approach has the advantage that it is the most accurate but is limited to systems containing a maximum of around one hundred atoms with currently available computing resources [17]. At the other extreme empirical potentials sacrifice accuracy for the advantage of speed which means that relatively large unit cells can be investigated. With the recent exception of Pettifor's bond order potentials [18, 19], we stress that all empirical potentials for silicon *assume* functional forms for the potential which are then fitted to experimental data such as the cohesive energy and bulk modulus. The theoretical arguments for the assumed functional forms are essentially classical in origin with little

0953-8984/90/5110259 + 30 $03.50

or no quantum mechanical basis. The arguments are based on distortions of bond length and angles from their ideal values and in some cases [12–14] intuitive estimates of how these distortions affect bond orders in the density matrix. If an empirical potential could be found which produces sensible minimum energy atomic configurations in a static calculation then there would be considerable scope for incorporating the potential in a simulation such as Monte Carlo (MC) or molecular dynamics in order to explore a greater area of configuration space and thereby seek the global minimum which, for an extensively reconstructed surface, may not be identified otherwise. The semi-empirical approach is a compromise in which the model supposedly still contains the essential physics yet the time consuming steps of the *ab initio* calculation, such as explicitly evaluative matrix elements of the Hamiltonian, are avoided by empirical parameterization.

In this paper we carry out static energy minimization calculations using a semi-empirical tight-binding approach called the tight-binding bond (TBB) model [20]. We assess the performance of the model by comparing the predictions of surface atomic structure with other experimental and theoretical work. Four silicon surfaces are investigated: Si(110)–1 × 1, Si(100)–2 × 1, Si(111)–2 × 1 and Si(113)–1 × 1.

Charge transfer between atoms in non-equivalent environments at a semiconductor surface might be expected because of incomplete screening of the ion cores resulting in a redistribution of electronic charge. If such a process does occur, then it is not clear what effect it is going to have on the atomic structure of the reconstructed surface. In addition, therefore, we address the question of whether such a charge transfer process must be considered explicitly in atomistic simulations of silicon surfaces.

Finally, we present static energy minimization calculations on the same four silicon surfaces using the empirical potential of Stillinger and Weber (SW) [11]. For the Si(100) and Si(111) surfaces, we have also incorporated the SW potential into a MC simulation of annealing. The aim is to show, in a comparative study, why the empirical SW potential does not perform well in predicting stable atomic structures for silicon surfaces.

2. Theoretical approaches

2.1. The tight-binding bond model

The TBB model [20], coupled with the self-consistency requirement of local charge neutrality (LCN), is the simplest semi-empirical tight-binding scheme for describing the energy of a system of atoms which is also consistent with the force theorem [21–23]. Moreover, it allows properties that depend on second-order charges in the energy, such as the elastic constants [20] and the heats of formation of alloys [24] to be calculated reliably. The TBB model has been discussed in detail by Sutton *et al* [20]. Here we confine ourselves to a brief summary of the model and the key differences between the TBB model and the more widely used band model (e.g. as used by Chadi [3–6] and Guo-Xin and Chadi [7]).

Starting with the Harris–Foulkes functional [25–26] of density functional theory [27, 28] it is possible [20] to express the binding energy of a solid in the following physically transparent form:

$$E_{\text{bind}} = Tr(\rho^{\text{out}} - \rho^{\text{f}})\mathbf{H} + \Delta E_{\text{xc}}[\rho^{\text{f}}] + \Delta E_{\text{es}}[\rho^{\text{f}}] + \Delta E_{\text{sp}} = E_{\text{cov}} + E_{\text{pro}} + \Delta E_{\text{xc}}[\rho^{\text{f}}] + \Delta E_{\text{es}}[\rho^{\delta}] + \Delta E_{\text{sp}}. \tag{1}$$

The electronic Hamiltonian **H** is constructed from an input charge density matrix ρ^{f}. ρ^{out} is the density matrix obtained from the eigenfunctions of **H**. Contact is made with tight-binding by assuming that a suitable choice of ρ^{f} is a superposition of atomic charge densities. When expanded in an atomic orbital basis, the corresponding density matrix, ρ^{f}, is then diagonal and the off-diagonal contributions to the trace in equation (1) arise only from the formation of bonds, as described by ρ^{out}. The off-diagonal elements contributing to the trace sum to the covalent bond energy E_{cov} while the sum of the diagonal elements defines the promotion energy E_{pro}. Equation (1) describes the energy change accompanying an impaginary process in which the solid is condensed from infinitely separated atoms. The promotion energy describes the sum of energies associated with individual atoms when the occupations of the atomic orbitals differ in the solid compared with the free atomic state. Note that the site-diagonal Hamiltonian matrix elements that appear in the promotion energy are those for the solid, and not those for the free atom. ΔE_{xc} and ΔE_{es} are the changes in the exchange-correlation and total electrostatic energies, respectively, as a result of the condensation. They are both functionals of the input charge density and may be apppoximated by a sum of pairwise interactions [20]. ΔE_{sp} accounts for the change in the spin–polarization energy associated with the condensation process; we assume that this quantity is a constant which does not depend on the atomic environment. The error in the binding energy (equation (1)), is of the order of $(\rho^{sc} - \rho^{f})(\rho^{sc} - \rho^{out})$, which ρ^{sc} is the Kohn–Sham self-consistent charge density.

In the TBB model the covalent bond energy and promotion energy are found by solving the Hamiltonian $\tilde{H}$ while the remaining terms in (1) are approximated by a sum of empirical pair potentials. Contact is made with the more commonly used band model by regrouping the terms in (1) and writing down the *total* energy as follows:

$$E_{total} = E_{bind} + E_{free\,atoms} = E_{band} - Tr\rho^{f}\mathbf{H} + \Delta H_{ex}[\rho^{f}] + \Delta E_{es}[\rho^{f}] + \Delta E_{sp}$$

$$+ E_{free\,atoms} = E_{band} + \left(E_{ii} - E_{ee} + E_{xc}[\rho^{f}] - \int \rho^{f}(\boldsymbol{r})\left(\frac{\delta E_{xc}}{\delta \rho^{f}(\boldsymbol{r})}\right) \mathrm{d}\boldsymbol{r}\right). \qquad (2)$$

The total energy is denoted by E_{total}, the energy of all the atoms in their free atomic state by $E_{free\,atoms}$, the ion–ion electrostatic energy by E_{ii} and E_{ee} is the electron–electron Coulomb energy. The band energy E_{band} is equal to $Tr\rho^{out}\mathbf{H}$. In the band model the total energy is represented by the band energy plus a sum of empirical repulsive pair potentials representing all the terms in large square brackets in equation (2).

If either (1) or (2) were solved exactly there would be no distinction between the band model and the TBB model apart from an unimportant shift in the energy zero equal to $E_{free\,atoms}$. The differences between these models arise because they are both approximations to the energy functions in equations (1) and (2). The empirical pair potentials in the two models represent physically different interaction energies. This is crucial if we now introduce some form of self-consistency into the electronic Hamiltonian. Properties that depend on second-order changes in the Hamiltonian require an explicit treatment of charge transfer effects, i.e. self-consistency. There are several simple schemes for introducing self-consistency into tight-binding models, and perhaps the simplest is to require LCN. This may be achieved by adjusting on-site Hamiltonian matrix elements. Physically, this amounts to assuming that electronic screening alters the local electrostatic potential at an atomic site so that the atom remains neutral.

The force theorem states that at the self-consistent charge distribution there is no contribution to the force on an atom arising from the self-consistent redistribution of

electronic charge. This is satisfied by the TBB model with LCN but not by the band model. it would also be satisfied by the band model if the cancellation between the change in the 'electron–electron double counting term' E_{ee} and the change in the site-diagonal contributions to the band energy were made explicitly. But this cancellation does not take place in the band model because E_{ee} is contained within the empirically fitted pair potential. By contrast, in the TBB model, the cancellation is made explicitly and there is no contribution to the force arising from the site-diagonal Hamiltonian matrix elements. Provided all atoms are locally charge neutral, the force on atom k in the x direction is given in the TBB model by

$$-\sum_{j\neq k}\sum_{\alpha\beta} 2\rho^{out}_{k\alpha j\beta}\frac{\partial \mathbf{H}_{j\beta k\alpha}}{\partial x_k}+\frac{\partial v(r_{jk})}{\partial x_k} \tag{3}$$

where $v(r)$ is the pair potential, r_{jk} is the length of the bond from atom k to a neighbouring atom j, and α and β denote orbital symmetries. Note that there are no site-diagonal contributions to the force in this expression, as required by the force theorem. LCN on atom i is achieved in the TBB model by varying all the Hamiltonian matrix elements $\mathbf{H}_{i\alpha i\alpha}$ by the same amount Δ_i. This assumption preserves the s–p splitting energy.

We point out that the covalent bond energy may be expressed in terms of the local density of states (LDOS), $n_{i\alpha}(E)$, as follows:

$$E_{cov}=\sum_{\substack{i\alpha\\ i\neq j}}\sum_{j\beta}\rho^{out}_{i\alpha j\beta}\mathbf{H}_{j\beta i\alpha}=\sum_{i\alpha}\int^{E_F}(E-\mathbf{H}_{i\alpha i\alpha})n_{i\alpha}(E)\,dE. \tag{4}$$

If i = j is included in the double sum in equation (4) we obtain instead the band energy. The integrand on the right-hand side then becomes $En_{i\alpha}(E)$. The intersite method (ISM) refers to calculations using the off-diagonal representation, while the site-diagonal method (SDM) uses only diagonal matrix elements. The equalities in equation (4) are exact provided the density matrix elements and local densities of states are exact. Thus, a comparison of the energies computed by the ISM and SDM provides a useful check on the calculation.

2.1.1. Parameterization of the model. The TBB model provides formal prescriptions for the force and energy in an assembly of atoms in terms of a localized atomic orbital basis. Nowhere are the matrix element integrals explicitly evaluated. Instead, an empirical parameterization of the model is carried out which is dependent on the system under investigation. The Hamiltonian matrix elements used in this study of silicon surfaces are the same as those used by Chadi [6] and Guo-Xin and Chadi [7], who obtained the empirical parameters by fitting the matrix elements to bulk properties of the silicon crystal for an sp^3 minimal basis set. Within the two-centre approximation, the length scaling of the off-diagonal Hamiltonian matrix elements is taken to be $1/(\text{distance})^2$ following Harrison [29]. This scaling law is truncated at a cut-off of 0.5 or 0.55 lattice parameters (LP), which lies between first- and second-neighbours in the ideal diamond crystal. The equilibrium lattice parameter is 5.341 Å. The angular dependence of the Hamiltonian matrix elements is taken from tables produced by Slater and Koster [30]. Non-orthogonality of the atomic orbital basis set provides a large repulsive energy contribution to the total promotion and bond energies. To first-order in the overlap this gives rise to a repulsive pair potential which actually dominates other contributions to the pair potential. Consequently, the pair potential is taken to be of the form A/r^4, where A is an empirical constant.

2.1.2. Computing minimum energy atomic configurations. We solve the Hamiltonian in real space using the recursion method [17, 31–33]. The recursion method enables matrix elements of the Greenian $\mathbf{G} = (E - \mathbf{H})^{-1}$ to be computed via a recursion algorithm and thereby the matrix elements of ρ^{out} according to

$$\rho^{\text{out}}_{i\alpha j\beta} = -\frac{2\text{Im}}{\pi}\int^{E_F} \mathbf{G}_{i\alpha j\beta}(E + i0^+)\,dE. \tag{5}$$

In the recursion method each Green function matrix element is represented by an infinite continued fraction. If all the levels of the continued fraction were calculated exactly, using the recursion algorithm, then the Greenian and hence the density matrix would be exact. This is impractical; instead, the infinite number of levels of the continued fraction beyond a certain point are approximated by a terminator. This means that the computed density matrix is inexact. The main advantage of the recursion method, however, is that it allows the effects of successive shells of neighbours to be studied systematically since the accuracy of ρ^{out} is determined by the number of exact levels (i.e. neighbour shells) used in the continued fraction before termination.

The position of the Fermi energy E_F is fixed at the perfect crystal value for the number of levels at which the calculation is done. So, for five levels, E_F is calculated by demanding that the five level LDOS gives four electrons per atom (in the case of silicon) when integrated up to E_F, where the LDOS on atom i is given by

$$n_i(E) = \sum_\alpha n_{i\alpha}(E) = -\frac{\text{Im}}{\pi}\sum_\alpha \mathbf{G}_{i\alpha i\alpha}(E + i0^+). \tag{6}$$

For calculations using up to eight levels in the recursion method we use a square root terminator for a single band. When determining the LDOS of an atom in a given atomic configuration to a large number of levels (e.g. 20) gaussian quadrature [34] is used instead. An extensive discussion of termination in the recursion method has appeared elsewhere [35].

All the necessary quantities for calculating the total energy and force on each atom are now known for a given atomic configuration. The forces are used in a variable metric minimization method [36] to compute a new atomic configuration and the cycle is repeated until the maximum displacement of any atom over one iteration is less than some arbitrary small amount [e.g. 5×10^{-6} LP]. This is a static energy minimization procedure. There is no guarantee that the algorithm produces the global minimum and the relaxed structure is highly dependent on the starting configuration. Therefore a number of calculations were made using different starting configurations for the four silicon surfaces investigated in this work.

We note that the methods of Chadi [3–6] and Guo-Xin and Chadi [7] are very similar to that described here, but differ in three principal ways. Firstly, we use the recursion method, rather than matrix diagonalization in $\boldsymbol{k}$ space, in order to solve the tight-binding Hamiltonian; secondly we impose LCN as a form of self-consistency whereas in Chadi's scheme there is no self-consistency and lastly the pair potentials are different.

2.1.3. Analysis of errors. There are errors in our tight-binding calculations from a variety of sources. Some of them stem from the use of an empirical parameterization of the energy functional described in equation (1). The use of a minimal basis set also introduces errors. The assumption that LCN is an adequate representation of self-consistency is another source. These errors are extremely difficult to quantify even if *ab initio* calculations were available for comparison. In this section we describe the errors that arise

Table 1. Perfect crystal values of the Fermi energy E_F (in eV), the cohesive energy per atom E_{coh} (in eV), and the parameter A (in eV Å^4) as a function of the number of recursion levels computed both by the intersite method (ISM) and the site-diagonal method (SDM) within the TBB model. The lattice parameter is 5.341 Å. In addition the dependence of the s–p mixing ratio SP_{mix} on the number of recursion levels is given (see section 2.1.4).

Levels	2	3	4	5	6	7	8
E_f^{ISM}	−0.205596	0.000359	0.080560	0.315072	0.297344	0.333416	0.381153
E_f^{SDM}	−0.155854	−0.042520	0.027728	0.308013	0.325486	0.331552	0.391135
E_{coh}^{ISM}	−5.468236	−4.794906	−4.736015	−4.803674	−4.792605	−4.780090	−4.770168
E_{coh}^{SDM}	−3.482315	−4.671071	−4.545900	−4.702427	−4.735065	−4.696694	−4.735542
SP_{mix}	1.538336	1.674317	1.697180	1.689129	1.697580	1.701196	1.704515
A^{ISM}	117.35285	115.11404	115.44143	115.99958	116.2712	116.27532	116.30106
A^{SDM}	113.02083	111.56384	116.39466	115.77384	115.80385	116.58478	116.24959

from the use of the recursion method to a small finite number of levels, since these errors are open to quantitative study.

When we say that the calculation has been performed to five recursion levels, we mean that five exact levels of the continued fraction have been computed using the recursion algorithm and the remainder have been approximated by a terminator. The errors we discuss in this section result from this use of a terminator in the continued fraction which causes the computed Green function matrix elements to be inexact.

Consider the equilibrium condition of the perfect diamond cubic crystal at 0 K. At the required lattice constant the total internal pressure, resulting from the covalent bond energy and the pair potential energy, must be zero [20]. This condition was used [37] to determine the parameter A in the pair potential. However, in evaluating the contribution to the pressure from the covalent bond energy, the recursion method was used to obtain the relevant off-diagonal Green function matrix elements. Then the imaginary parts of these approximate Green function matrix elements were integrated up to the Fermi energy in order to obtain the off-diagonal density matrix elements (see equation (5)) that appear in the covalent bond energy, equation (4). As described in section 2.1.3, the Fermi energy is determined by integrating the imaginary part of the approximate diagonal Green function matrix elements until each atom is asociated with four electrons. It follows that the Fermi energy and the parameter A are dependent on the number of recursion levels because of the inexactness of the continued fraction representations of the Green function matrix elements. Thus, the binding energy per atom and the s–p mixing (defined by Paxton and Sutton [17] as the ratio of the occupancy of p-states to s-states on an atom) in the ideal crystal are also dependent on the number of levels for the same reasons. These dependencies are summarized in table 1.

We have already pointed out (see equation (2.4)) that there are two methods for computing the sum of the covalent bond and promotion energies: the SDM and ISM. If the Green function matrix elements were exact, these methods would yield identical results. The discrepancies between the energies obtained by these methods is therefore some indication of the magnitude of the errors incurred by using the recursion method. However, it is important to bear in mind that in this work as in [17] and [37], we are using the matrix formulation of the recursion method [38], as modified by Paxton *et al* [37]. When we evaluate the covalent bond and promotion energies in the SDM, we do so by considering all four orbitals on each atom at a time, which results in a continued fraction

of 4×4 matrices. When we use the ISM, however, we consider the four orbitals on each of the neighbouring atoms of a bonded pair and evaluate a continued fraction of 8×8 matrices. There is, therefore, a difference in the Fermi energy evaluated by the two methods, for the same number of exact recursion levels. This difference in the Fermi energies in the ISM and SDM calculations leads to different A parameters and binding energies per atom. That is why both sets of parameters are listed in table 1. The fact that, for the same number of recursion levels, the A parameters are different has an important consequence. It means that the SSDM and ISM energy functionals are not identical, not only because of the differences in the covalent bond and promotion energies, but also because the pair potential contributions are different. In this sense, we should regard the SDM and ISM representations as distinct energy functionals. When we carry out a static energy minimization, using equation (3) for the forces, we are, strictly speaking, minimizing the ISM energy functional and not the SDM energy functional.

Because the SDM and ISM representations are really distinct functionals, we believe that a comparison of their energies exaggerates the errors of the recursion method. To obtain a more realistic estimate, we pose a slightly different question. Since the forces and energies may both be computed within the ISM we should estimate the errors arising from a finite number of recursion levels within the ISM only. To do this we recall that as the number of exact levels in the continued fraction tends to infinity the ISM becomes exact. We have therefore carried out a systematic series of calculations for the same surface (Si(110)–1×1) using the ISM between two and eight exact recursion levels. The aim is to see whether the atomic structure and the surface binding energy converge uniformly as a function of the number of exact levels, and to estimate the errors at a given number of levels. These calculations are described in section 3.1.2.

2.2. *The Stillinger–Weber potential*

The SW potential [11] assumes that the behaviour of silicon is adequately described by a combination of pair and three-body potentials $v_2(\mathrm{i}, \mathrm{j})$ and $v_3(\mathrm{i}, \mathrm{j}, \mathrm{k})$ where the total potential energy Φ is given by

$$\Phi = \sum_{\substack{\mathrm{ij} \\ \mathrm{i}<\mathrm{j}}} v_2(\mathrm{i}, \mathrm{j}) + \sum_{\substack{\mathrm{ijk} \\ \mathrm{i}<\mathrm{j}<\mathrm{k}}} v_3(\mathrm{i}, \mathrm{j}, \mathrm{k}) \tag{7}$$

with the i, j and k indices corresponding to different atoms. Energy and length parameters ε and σ are then introduced so that v_2 and v_3 may be written in the form

$$v_2(r_{\mathrm{ij}}) = \varepsilon f_2(r_{\mathrm{ij}}/\sigma) \tag{8}$$

and

$$v_3(\boldsymbol{r}_\mathrm{i}, \boldsymbol{r}_\mathrm{j}, \boldsymbol{r}_\mathrm{k}) = \varepsilon f_3(\boldsymbol{r}_\mathrm{i}/\sigma, \boldsymbol{r}_\mathrm{j}/\sigma, \boldsymbol{r}_\mathrm{k}/\sigma) \tag{9}$$

where

$$f_2(r) = \begin{cases} A(Br^{-p} - r^{-q}) \exp[(r-a)^{-1}] & (r < a) \\ 0 & (r \geqslant a) \end{cases} \tag{10}$$

$$f_3(\boldsymbol{r}_\mathrm{i}, \boldsymbol{r}_\mathrm{j}, \boldsymbol{r}_\mathrm{k}) = h(r_{\mathrm{ij}}, r_{\mathrm{ik}}, \theta_{\mathrm{jik}}) + h(r_{\mathrm{ji}}, r_{\mathrm{jk}}, \theta_{\mathrm{ijk}}) + h(r_{\mathrm{ki}}, r_{\mathrm{kj}}, \theta_{\mathrm{ikj}}) \tag{11}$$

$$h(r_{ij}, r_{ik}, \theta_{jik}) = \lambda \exp[\gamma(r_{ij} - a)^{-1} + \gamma(r_{ik} - a)^{-1}](\cos\theta_{jik} + \tfrac{1}{3})^2. \quad (12)$$

The parameter set is as follows:

$A = 7.049556277$ $B = 0.6022245584$

$p = 4$ $q = 0$ $a = 1.80$

$\lambda = 21.0$ $\gamma = 1.20$

which fixes ε and σ if the potential is to predict the correct cohesive energy and density for Si at 0 K. It turns out that $\sigma = 2.0951$ Å and $\varepsilon = 1.0836$ eV per atom.

2.2.1. Static energy minimizations. We calculate that the equilibrium lattice parameter for the SW potential at 0 K is 5.431 Å in agreement with Dodson [39]. Some care is needed if the total force on an atom is to be written as a sum of bond forces due to neighbouring atoms. The reader is referred to the appendix for details of how this decomposition is achieved. The resulting force expression together with the above prescription for the energy have been incorporated into the same variable metric minimization procedure that is used in the tight-binding relaxation in order to perform static energy minimizations with the SW potential.

2.2.2. Monte Carlo simulated annealing. Reaching the optimum relaxed atomic configuration from the static energy calculation described above presupposes a starting configuration somewhere in the correct energy well. In order to try and overcome the possible confinement to a local, rather than a global, minimum, we have incorporated the SW potential into an MC simulation of annealing [40]. The simulation models consist of blocks of ten layers of atoms. Born-von Karman boundary conditions reproduce the block infinitely in the plane of the surface. For the Si(111) surface, each layer contains sixteen Si atoms and the top four layers were placed initially in the Pandey π-bonded chain configuration [41–43]. For the Si(100) surface, the block contains 160 atoms per layer. The MC temperature parameter was set to 2500 K. This temperature resulted in disorder in the surface layers but the bulk did not melt. Each atom in turn was then moved 0.04 LP (fixed throughout the run) in a random direction, a value chosen to give an initial acceptance rate of ~20%. The resulting energy change was used in the standard MC criterion for accepting or rejecting a move. By reducing the temperature, by 2.5 K for Si(111) or by 2 K for Si(100), every tenth cycle through all the atoms, the temperature was eventually brought to below 100 K. The process was repeated several times to ensure that the relaxed structures were reproduced.

3. Results

3.1. The TBB Model

For the bulk terminated and energy minimized surfaces investigated in this work, the ISM and SDM surface binding energies relative to the perfect crystal are summarized in

Table 2. ISM and SDM energies (in mJ m^{-2}) for the bulk terminated and relaxed surfaces according to the TBB model with local charge neutrality.

Surface	Recursion levels	ISM energy (ideal)	ISM energy (relaxed)	SDM energy (ideal)	SDM energy (relaxed)
Si(110)–(1 × 1)	5	1750	1573	1376	1383
Si(100)–(2 × 1)	8	1774	1343	1623	1270
Si(111)–(2 × 1)	7	1437	1413	1226	1286
Si(113)–(1 × 1)	6	1864	1378	1581	1116

table 2. Note that for the Si(100)–2 × 1, Si(111)–2 × 1 and Si(113)–1 × 1 surfaces, all calculations have been performed with LCN; for the Si(110)–1 × 1 surface we present calculations both with and without imposing LCN.

3.1.1. Position of the Fermi energy. The LDOS for a Si atom in the perfect crystal calculated to 5, 6, 7 and 8 levels of the recursion method using a single band square-root terminator is shown in figure 1 with the twenty level LDOS calculated with Gaussian quadrature for comparison. In each case the position of the Fermi energy calculated to the corresponding number of levels is marked by a vertical line. We find that the Fermi energy is always in the band gap. The actual values can be found in the figure caption. It is noted that if the LDOS were calculated exactly, then the Fermi energy would be at the top of the valence band, i.e. at 0 eV.

3.1.2. The Si(110)–1 × 1 surface. The ideal and relaxed surfaces are shown in figure 2. We find that static energy minimization with LCN to five recursion levels and a Hamiltonian range of 0.5 LP results in no relaxation taking place along the $(1\bar{1}0]$ direction. Following Chadi [5], we can characterize the stable reconstruction by a tilt angle θ defined as

$$\theta = |\tan^{-1}(z_{12}/x_{12})| \tag{13}$$

where the x- and z-axes have been defined in figure 2 and x_{12} (z_{12}) is the difference in the x (z) coordinates of nearest neighbour atoms at the surface. We find that $\theta = 31.3°$. The relaxed surface was obtained by giving the two surface atoms initial displacements in z of ± 0.02 LP. The final displacements from the ideal positions are given in table 3 together with the values of Δ_i for the five level relaxation.

When LCN is switched off, relaxation of the same starting configuration to five levels (with an ISM energy of 1855 mJ m^{-2}) results in an unbuckled surface very similar to the ideal surface shown in figure 2(*a*) with a final ISM energy of 1782 mJ m^{-2}. This metastable surface could *not* be found when LCN was reimposed. For an initial displacement in z of ± 0.05 LP, however, relaxation to five levels without LCN results in an energy minimized structure similar to that in figure 2(*b*) but with $\theta = 29.0$ °C and an ISM energy of 1477 mJ m^{-2}. The ISM energy of the $\theta = 29.0°$ structure differs from the ISM energy of the $\theta = 31.3°$ structure by only 6.1%. Final displacements are in table 3.

A breakdown of the surface binding energy into the promotion energy, the covalent bond energy and the pair potential energy contributions is given in table 4 for the ideal and $\theta = 31.3°$ structures. By comparing the changes in these energy terms which occur due to relaxation, we find that the lowering in the surface binding energy is due to the

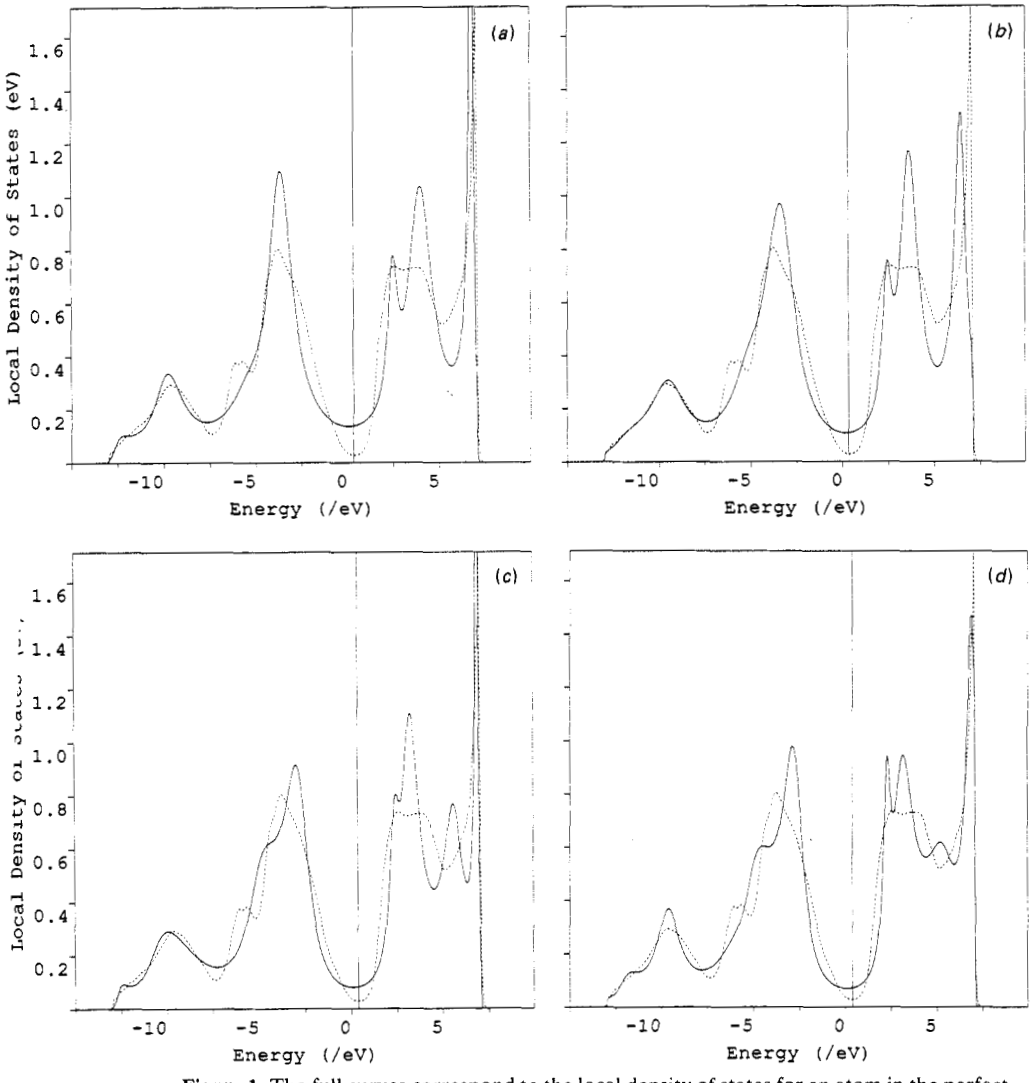

Figure 1. The full curves correspond to the local density of states for an atom in the perfect crystal calculated to (*a*) 5, (*b*) 6, (*c*) 7 and (*d*) 8 levels of the recursion method using a single square-root terminator. The position of the Fermi energy E_F is marked by a vertical full line. The actual values of E_F (in eV) are 0.325, 0.332, 0.391 and 0.392, respectively, for (*a*)–(*d*). The broken curve in each case corresponds to the local density of states of an atom in the perfect crystal calculated to 20 recursion levels using Gaussian quadrature. It is included in order to emphasise that, at the relatively small number of levels at which the static energy minimization calculations are performed, the non-zero local density of states around E_F results in E_F being placed in the middle of the band gap.

reduction in the promotion energy and the pair potential energy contributions; we find that the tilting of the surface chains of atoms is not driven by a lowering in the covalent bond energy. A summary of the individual bond energy changes for the $\theta = 31.3°$ structure relative to the ideal surface is provided in table 5.

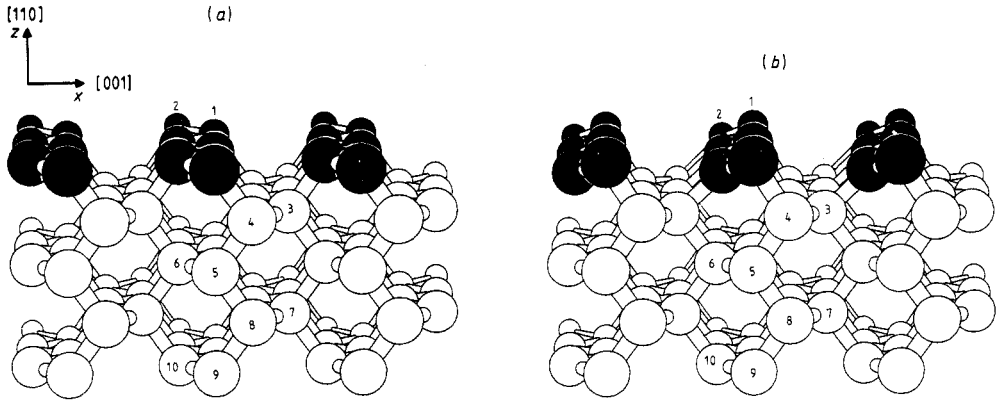

Figure 2. (*a*) The bulk terminated Si(110) surface along the $(1\bar{1}0]$ direction. (*b*) The Si(110)–1×1 surface after relaxation with the tight-binding bond model. With local charge neutrality, the tilt angle $\theta = 31.3°$. Without local charge neutrality, the tilt angle $\theta = 29.0°$. Numbers correspond to atom indices (see tables and text).

Table 3. Final atomic displacements in lattice parameter units for the Si(110)–1×1 surface, according to the TBB model, after being relaxed self-consistently and non-self-consistently to give the buckled $\theta = 31.3°$ and $\theta = 29.0°$ structures, respectively. For the $\theta = 31.3°$ structure the rigid shifts in the on-site Hamiltonian matrix elements Δ_i required to satisfy LCN are given in eV. The relaxed surface and atom numbers are shown in figure 2.

	$\theta = 31°$			$\theta = 29°$	
Atom number, i	Δx_i	Δz_i	Δ_i	Δx_i	Δz_i
1	1.00×10^{-2}	5.61×10^{-2}	0.910	2.56×10^{-2}	5.18×10^{-2}
2	4.63×10^{-2}	-7.20×10^{-2}	−0.080	5.57×10^{-2}	-7.03×10^{-2}
3	-8.87×10^{-3}	-1.25×10^{-2}	0.074	-5.16×10^{-3}	-9.57×10^{-3}
4	-2.52×10^{-3}	2.26×10^{-2}	0.286	3.87×10^{-4}	1.84×10^{-2}
5	8.59×10^{-4}	9.96×10^{-3}	0.077	-4.26×10^{-4}	8.10×10^{-3}
6	-5.36×10^{-4}	-7.37×10^{-3}	0.073	-1.30×10^{-3}	-6.30×10^{-3}
7	-1.06×10^{-4}	-3.88×10^{-3}	0.040	-3.55×10^{-4}	-3.46×10^{-3}
8	-3.96×10^{-4}	4.24×10^{-3}	0.029	-4.26×10^{-4}	3.69×10^{-3}
9	1.65×10^{-4}	1.90×10^{-3}	0.011	1.24×10^{-4}	1.67×10^{-3}
10	5.88×10^{-5}	-2.09×10^{-3}	0.013	1.61×10^{-4}	-1.70×10^{-3}

Finally, in figure 3 we present the results of the systematic study described in section 2.1.4. We find that both the atomic structure and the ISM surface energy converge as a function of the number of recursion levels. We estimate the errors in the ISM energies at 5, 6, 7 and 8 levels from these calculations to be ± 50 mJ m^{-2}, i.e. $\pm 3\%$, and the errors in the atomic structure at 5, 6, 7 and 8 levels to be $\pm\frac{1}{2}°$, i.e. $\pm 2\%$. These errors are with respect to an exact solution of the model Hamiltonian.

3.1.3. The Si(100)–2 × 1 surface. The two surface atoms of the bulk terminated surface (figure 4(*a*)) were pinched together by displacing them by a small amount along [011]. This starting configuration was then relaxed with LCN to eight recursion levels and a

Table 4. Breakdown of the surface binding energy into the promotion energy E_{pro}, the covalent bond energy E_{cov}, and the pair potential energy E_{pp} for each of the surfaces studied with the TBB model. The 'Difference' row gives the differences between the relaxed surface and the reference configuration. In each case local charge neutrality has been imposed to ensure global charge conservation. All energies are given in eV.

Surface	E_{prom}	E_{cov}	E_{pp}
Ideal 110	44.1310	−218.658	109.478
Relaxed 110	43.0059	−217.154	108.877
Difference	−1.1251	+1.504	−0.601
Unbuckled 100	45.4278	−218.320	108.572
Relaxed 100	44.9371	−219.104	109.775
Difference	−0.6336	−0.784	+1.203
Untilted 111	65.4796	−315.058	156.243
Relaxed 111	64.2650	−314.282	156.594
Difference	−1.2146	+0.776	+0.351
Ideal 113	92.4982	−462.433	231.662
Relaxed 113	94.1585	−462.896	229.030
Difference	+1.6603	−0.463	−2.632

Table 5. Breakdown of the bond energy for the relaxed Si(110)–1 × 1 surface into the ssσ, spσ, ppσ and ppπ components for each bond in the surface region identified by the atom number of the atom at either end of the bond. E_{ij} is the total covalent bond energy between atom i and atom j. All energies are in eV and represent the *change* relative to the corresponding bond in the idal surface. Atom numbers are given in figure 2. This analysis gives a picture of the local chemistry. In particular it demonstrates that despite a strengthening in the back-bonds to atom 2 as a result of tilting, the back-bonds to atom 1 are weakened by a greater amount (see text).

Atom i	Atom j	$\Delta E_{ss\sigma}$	$\Delta E_{sp\sigma}$	$\Delta E_{pp\sigma}$	$\Delta E_{pp\pi}$	ΔE_{ij}
1	2	0.431	0.209	−0.144	−0.047	0.449
2	3	−0.156	−0.137	−0.866	−0.201	−1.360
1	4	0.355	0.888	0.637	0.505	2.385
3	4	0.035	−0.033	−0.099	−0.059	−0.155
4	5	0.123	0.227	0.297	0.047	0.694
3	6	0.039	0.119	0.082	0.059	0.299
5	6	0.036	0.048	0.032	0.002	0.119
6	7	−0.023	−0.065	−0.160	−0.044	−0.292
5	8	0.053	0.111	0.187	0.028	0.379
7	8	0.006	0.011	0.010	0.001	0.027
8	9	0.021	0.043	0.071	0.009	0.144
7	10	−0.018	−0.037	−0.052	−0.011	−0.118
9	10	0.001	0.003	0.003	0.001	0.008

Hamiltonian range of 0.55 LP. The final relaxed configuration is shown in figure 4(*b*) and consists of asymmetric buckled dimers. Final displacements relative to the ideal surface are given in table 6. There is no significant relaxation along the [0$\bar{1}$1] direction. Table 6

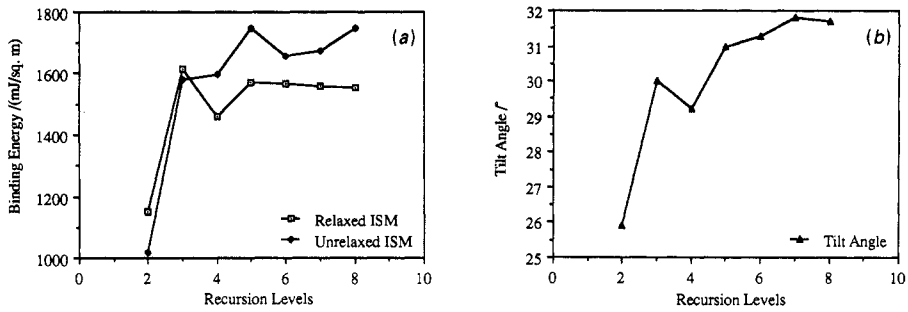

Figure 3. (*a*) Systematic study of the ISM energy for the Si(110)–1 × 1 surface relaxed with local charge neutrality as a function of the number of recursion levels. (*b*) Variation of the tilt angle characterising the atomic structure of the relaxed Si(110)–1 × 1 surface with the number of recursion levels (see text).

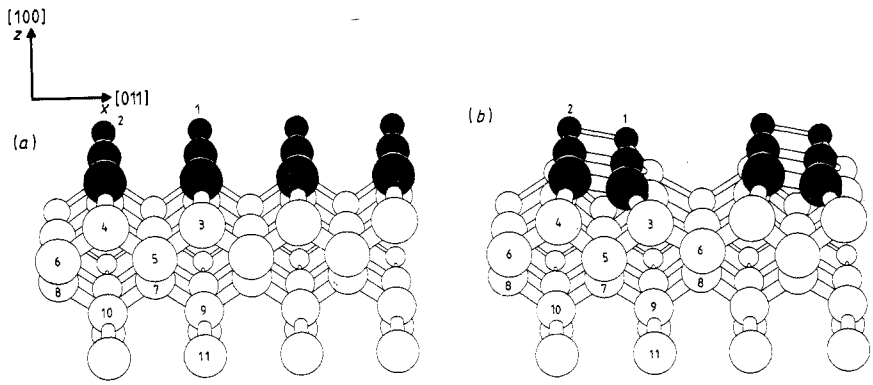

Figure 4. (*a*) The bulk terminated Si(100) surface along the [0$\bar{1}$1] direction. (*b*) The Si(100)–(2 × 1) surface after relaxation with the tight-binding bond model. The surface has adopted an asymmetric buckled dimer reconstruction.

also contains the Δ_i values calculated to eight levels. In addition we find that a symmetric unbuckled dimer configuration obtained from a relaxation using the Stillinger–Weber potential has an ISM energy of 1383 mJ m^{-2}, calculated with LCN, eight recursion levels and a Hamiltonian range of 0.55 LP. This is very close to the value of 1343 mJ m^{-2} listed in table 2 for the asymmetric buckled dimer surface. Given the three per cent error in our calculated energies, we cannot distinguish between these two reconstructions. The final atom displacements and Δ_i values for the symmetric dimer surface are also given in table 6.

A breakdown of the surface binding energy is given in table 4 for both relaxed structures. We find that tilting of the surface dimers is accompanied by a reduction in the promotion energy and the covalent bond energy but that these reductions are almost exactly compensated by an increase in the pair potential energy. The changes in the individual bond energies between the symmetric dimer surface obtained from the Stillinger–Weber relaxation and the asymmetric buckled dimer structure are summarized in table 7.

Table 6. Final atomic displacements in lattice parameter units for the Si(100)–2 × 1 surface, after being relaxed self-consistently with the TBB model, together with the rigid shifts in the on-site Hamiltonian matrix elements Δ_i required to ensure LCN (in eV). The relaxed surface and atom numbers are shown in figure 4. Corresponding values for the symmetric dimer surface are given in brackets.

Atom number i	Δx_i	Δz_i	Δ_i
1	-1.79×10^{-1}	-8.45×10^{-2}	−0.096
	(-1.32×10^{-1})	(-1.72×10^{-2})	(0.683)
2	1.10×10^{-1}	2.61×10^{-3}	0.867
	(1.32×10^{-1})	(1.73×10^{-2})	(0.681)
3	-1.23×10^{-2}	-4.46×10^{-3}	0.071
	(-2.12×10^{-2})	(3.57×10^{-3})	(0.568)
4	2.39×10^{-2}	1.64×10^{-2}	0.504
	(2.12×10^{-2})	(3.57×10^{-3})	(0.567)
5	-2.88×10^{-4}	-2.24×10^{-2}	0.345
	(5.49×10^{-5})	(-2.03×10^{-2})	(0.435)
6	1.32×10^{-2}	2.55×10^{-2}	−0.078
	(3.06×10^{-5})	(2.05×10^{-2})	(0.120)
7	-2.13×10^{-3}	-1.30×10^{-2}	0.190
	(-2.68×10^{-5})	(-1.31×10^{-2})	(0.268)
8	1.73×10^{-3}	1.55×10^{-2}	0.019
	(-2.40×10^{-5})	(1.33×10^{-2})	(0.118)
9	3.91×10^{-3}	1.99×10^{-3}	0.053
	(6.18×10^{-3})	(3.72×10^{-5})	(0.119)
10	-5.78×10^{-3}	-1.21×10^{-3}	0.065
	(-6.23×10^{-3})	(-8.11×10^{-6})	(0.119)

Table 7. Breakdown of the bond energy for the relaxed Si(100)–2 × 1 surface similar to that in table 5. Each entry represents the change relative to the corresponding bond in the untilted symmetric dimer reconstruction obtained from a relaxation using the Stillinger–Weber potential. Atom numbers are given in figure 4. This analysis enables the contributions to the lowering in the covalent bond energy on tilting to be identified.

Atom i	Atom j	$\Delta E_{ss\sigma}$	$\Delta E_{sp\sigma}$	$\Delta E_{pp\sigma}$	$\Delta E_{pp\pi}$	ΔE_{ij}
1	2	0.254	−0.742	0.317	−0.536	−0.707
1	3	−0.121	−0.384	−0.300	−0.249	−1.054
2	4	0.117	0.038	−0.190	0.065	0.030
3	5	0.119	0.460	0.082	−0.019	0.642
4	5	0.141	0.040	0.446	0.115	0.742
3	6	−0.050	−0.136	0.081	−0.003	−0.108
4	6	−0.015	−0.060	−0.207	−0.083	−0.365
5	7	−0.010	−0.029	−0.067	−0.031	−0.137
6	8	0.023	0.050	0.061	0.018	0.152
7	9	−0.015	−0.028	−0.050	−0.010	−0.103
8	9	0.024	0.072	0.168	0.030	0.295
7	10	−0.012	−0.033	−0.039	−0.011	−0.095
8	10	0.028	0.044	0.015	0.009	0.096
9	11	0.008	0.013	0.013	0.003	0.038

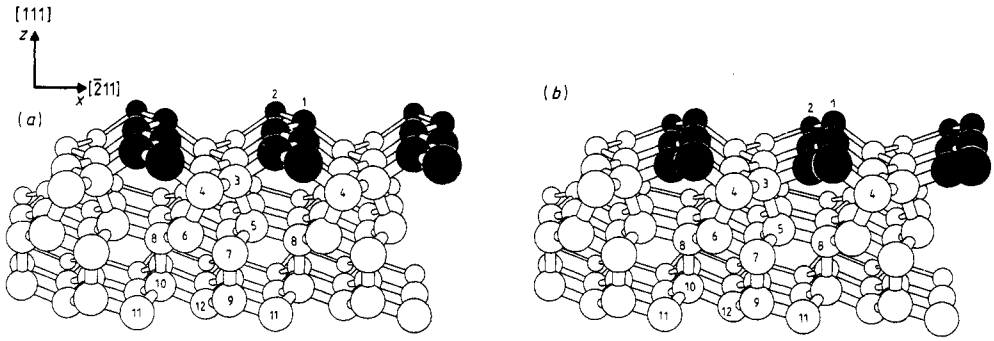

Figure 5. (*a*) The Pandey π-bonded chain reconstruction for the Si(111)–2 × 1 surface along the [0$\bar{1}$1] direction; this was the starting configuration for the tight-binding relaxation. (*b*) The Si(111)–(2 × 1) surface after relaxation with the tight-binding bond model. The surface atoms (shaded) have been tilted by 30.4°.

Table 8. Final atomic displacements in lattice parameter units for the Si(111)–2 × 1 surface, after being relaxed self-consistently with the TBB model, together with the rigid shifts in the on-site Hamiltonian matrix elements Δ_i required to ensure LCN (in eV). The relaxed surface and atom numbers are shown in figure 5.

Atom number i	Δx_i	Δz_i	Δ_i
1	1.67×10^{-1}	4.68×10^{-4}	0.039
2	5.71×10^{-1}	1.23×10^{-1}	0.606
3	-1.88×10^{-1}	-8.21×10^{-3}	0.164
4	1.65×10^{-1}	-1.82×10^{-2}	0.120
5	-2.25×10^{-2}	2.21×10^{-3}	0.225
6	1.82×10^{-2}	3.09×10^{-3}	0.277
7	4.98×10^{-4}	-2.36×10^{-2}	0.362
8	-1.47×10^{-3}	2.77×10^{-2}	0.046
9	1.00×10^{-3}	-1.34×10^{-2}	0.137
10	-1.42×10^{-3}	1.44×10^{-2}	0.093

3.1.4. The Si(111)–2 × 1 surface. We constructed the π-bonded chain model of this surface suggested by Pandey [41–43] and shown in figure 5(*a*). It has an ISM energy of 1470 mJ m^{-2}. We find that relaxation with LCN to seven recursion levels and a Hamiltonian range of 0.55 LP results in the π-bonded chains becoming tilted with a tilt angle of 30.4° relative to the starting configuration. The relaxed surface is shown in figure 5(*b*). In table 8 we present the final atom displacements from the ideal structure. No significant relaxation takes place along the [0$\bar{1}$1] direction. Table 8 also contains the Δ_i values calculated to seven levels.

A breakdown of the surface binding energy is given in table 4 for the relaxed structure; in addition we give the breakdown for the untilted π-bonded chain model shown in figure 5(*a*). We find that the tilting of the surface π-bonded chains is driven by a reduction in the promotion energy. A breakdown of the individual bond energies of the relaxed structure relative to the untilted configuration is given in table 9.

Table 9. Breakdown of the bond energy for the relaxed Si(111)–2 × 1 surface similar to that in table 5. Each entry represents the change relative to the corresponding bond in the untilted π-bonded chain surface. Atom numbers are given in figure 5.

Atom i	Atom j	$\Delta E_{ss\sigma}$	$\Delta E_{sp\sigma}$	$\Delta E_{cc\sigma}$	$\Delta E_{pp\pi}$	ΔE_{ij}
1	2	0.605	−0.144	−0.230	0.076	0.307
2	3	0.369	0.552	−0.455	0.282	0.748
1	4	0.167	0.161	−0.698	−0.043	−0.412
3	4	−0.060	−0.131	−0.048	−0.069	−0.308
3	5	0.161	0.318	0.505	0.155	1.139
4	6	0.008	0.114	−0.324	0.070	−0.132
5	7	0.001	0.001	−0.011	−0.012	−0.021
6	7	−0.099	−0.175	−0.220	−0.079	−0.573
5	8	0.058	0.139	0.220	0.032	0.448
6	8	0.019	0.048	0.008	0.000	0.075
7	9	−0.081	−0.159	−0.158	−0.058	−0.455
8	10	0.103	0.203	0.235	0.064	0.605
9	11	−0.023	−0.044	−0.071	−0.020	−0.158
10	11	0.008	0.012	−0.002	−0.008	0.010
9	12	0.004	0.011	0.015	0.006	0.036
10	12	0.033	0.066	0.091	0.019	0.209

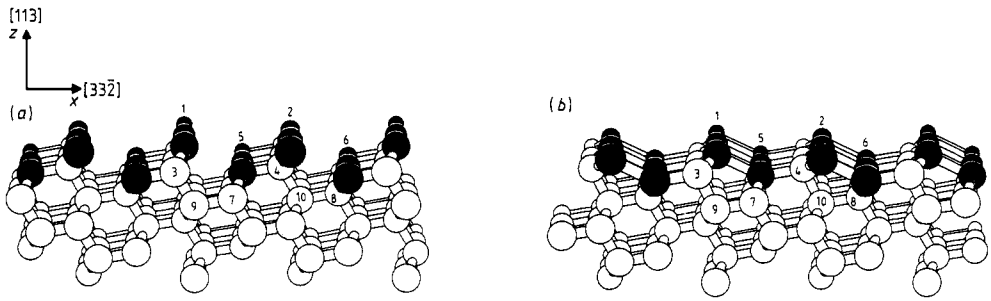

Figure 6. (*a*) The bulk terminated Si(113) surface along the [$\bar{1}$10] direction. (*b*) The Si(113)–1 × 1 surface after relaxation with the tight-binding bond model. The surface has adopted a 'rebonding at steps' reconstruction.

3.1.5. The Si(113)–1 × 1 surface. We reconstructed the ideal surface shown in figure 6(*a*) by pinching together the twofold coordinated atom at the surface with an atom in the same sublattice but in the second layer down to give a 1 × 1 periodicity. This rebonding at steps reconstruction leads to a 66.7% reduction in the density of dangling bonds. Relaxation with LCN to six recursion levels and a Hamiltonian range of 0.55 LP results in the newly formed bonds springing apart. Once this occurs, the distance between atom 1 and atom 5 and the distance between atom 2 and atom 6 (see figure 6(*a*)) both exceed the Hamiltonian range and the bond is never reformed. We therefore repeated the relaxation with the same starting configuration but with a Hamiltonian range of 0.6 LP. This still lies between first and second neighbours in the perfect crystal. We find that the rebonding at steps reconstruction shown in figure 6(*b*) is stable, but that the final bond lengths between atom 1 and atom 5 and between atom 2 and atom 6 are

Table 10. Final atomic displacements in lattice parameter units for the Si(113)–1 × 1 surface, after being relaxed self-consistently with the TBB model, together with the rigid shifts in the on-site Hamiltonian matrix elements Δ_i, required to ensure LCN (in eV). The relaxed surface and atom numbers are shown in figure 6.

Atom number i	Δx_i	Δz_i	Δ_i
1	1.18×10^{-1}	-3.18×10^{-2}	0.466
2	1.17×10^{-1}	-3.02×10^{-2}	0.471
3	1.68×10^{-2}	2.31×10^{-2}	0.616
4	1.64×10^{-2}	2.34×10^{-2}	0.618
5	-3.33×10^{-2}	1.57×10^{-2}	0.385
6	-3.26×10^{-2}	1.65×10^{-2}	0.388
7	2.34×10^{-3}	-2.83×10^{-4}	0.478
8	2.55×10^{-3}	5.45×10^{-4}	0.477
9	-1.69×10^{-3}	1.79×10^{-3}	0.356
10	-1.63×10^{-3}	2.32×10^{-3}	0.354

Table 11. Energies (in mJ m^{-2}) of the bulk-terminated surfaces investigated in the present work according to the Stillinger–Weber potential together with the energies after relaxation. Note that for Si(110)–1 × 1 and Si(111)–2 × 1, the relaxed surface is the bulk-terminated surface according to the Stillinger–Weber potential.

Surface	Unrelaxed energy	Relaxed energy
Si(110)–(1 × 1)	1721	1721
Si(100)–(2 × 1)	2434	1489
Si(111)–(2 × 1)	1405	1405
Si(113)–(1 × 1)	2201	1640

stretched by 27.1% and 27.6%, respectively, relative to a bond in the perfect crystal. The final displacements relative to the ideal surface are given in table 10 together with the values calculated to six levels. There is no significant relaxation along the [$\bar{1}$10] direction.

Table 4 contains the breakdown of the surface binding energy for the ideal and relaxed structures. We find that the stability of the relaxed surface is controlled both by a reduction in the covalent bond energy and a reduction in the pair potential energy.

3.2. The SW potential

We calculate the range of interaction of the SW potential to be 0.694 LP. The energies of the ideal bulk terminated surfaces as well as the final energies of the relaxed surfaces according to the SW potential are given in table 11.

In the case of the Si(110)–1 × 1 surface, we find that static minimization predicts no buckling of the surface chains. Furthermore, the effect of relaxation on even an extensively reconstructed set of coordinates is to move all the atoms back to their bulk terminated positions unless an atom is moved beyond the range of interaction of the potential in which case an ideal vacancy results.

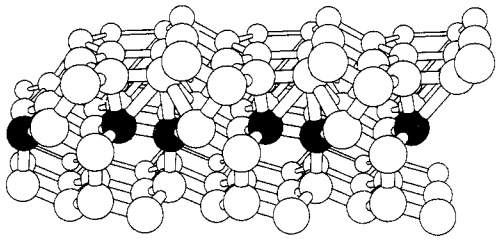

Figure 7. One of the two metastable surfaces for Si(111)–2 × 1 found by the Stillinger–Weber potential. Shaded atoms have five neighbours. The other metastable surface closely resembles the untilted π-bonded chain configuration shown in figure 5(*a*).

For the Si(100) surface, if the two surface atoms are moved so that they are less than 0.694 LP apart, we find by static minimization that an untilted symmetric dimer reconstruction is a stable configuration. We stress that in the static calculation we have limited ourselves to a 2 × 1 surface unit cell. We have confirmed by MC simulated annealing that untilted symmetric dimers are preferred, but find that dimerization *is* accompanied by a substantial number of defects.

When the Pandey π-bonded chain reconstruction of the Si(111)–2 × 1 surface is made the starting configuration for the static minimization, we find that both an untilted chain configuration (similar to figure 5(*a*)) and a structure involving fivefold coordinated atoms (figure 7) are stable structures with energies of 1858 mJ m^{-2} and 1853 mJ m^{-2}, respectively. Both of these are metastable, however, since they have higher energies than the ideal bulk terminated Si(111) surface (see table 11). In the MC simulation we have confirmed that the Pandey π-bonded chain configuration is returned to the ideal bulk terminated surface after simulated annealing with this potential. Initially, the surface became highly disordered in appearance. As the temperature fell, the atoms were returned to their bulk terminated positions. The bulk structure resulted after every run, although, as figure 8 shows, there is sometimes some disorder present, probably due to cooling too rapidly.

In the case of the Si(113)–1 × 1 surface, we find by static minimization that the SW potential predicts the rebonding at steps reconstruction to be stable. The final atomic structure is very similar to the TBB model result (figure 6(*b*)).

4. Discussion

4.1. The TBB model

4.1.1. Position of the Fermi energy. As explained in section 2.1.3, the Fermi energy is fixed at the perfect crystal value for the number of recursion levels at which the static minimization calculation is performed. If the density matrix were computed accurately, the Fermi energy would be fixed at the top of the valence band, since there are no dangling bonds and hence no electronic states in the band gap of the perfect crystal. By fixing the Fermi energy to be the same as that of the perfect crystal we do not allow the Fermi energy to re-adjust in the presence of the surface. Since the difference in the exact Fermi energies for the perfect crystal and the semi-infinite crystal is approximately half the band gap, we make an increasing error in the Fermi energy for the semi-infinite crystal as the number of recursion levels increases. However, we have shown in figure 1 that to 5, 6, 7 and 8 recursion levels (the numbers used in subsequent calculations) the perfect crystal LDOS is non-zero in the band gap region. This is because the calculated density matrix is not exact. As can be seen, this has the effect of placing the Fermi energy

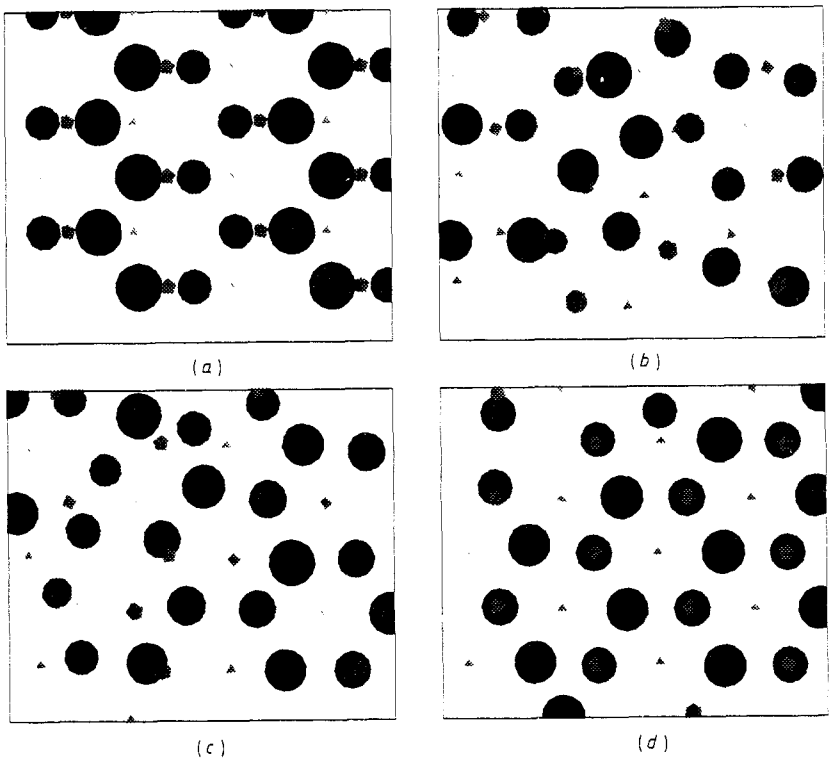

Figure 8. Monte Carlo simulated anneal of the Si(111) surface using the Stillinger–Weber potential. The surface is viewed from above, with the larger circles representing atoms nearer the surface. The Pandey π-bonded chain structure (large atoms) is shown in (*a*). Annealed configurations are shown at (*b*) 2000 K and (*c*) 1700 K. In (*d*), at 100 K, most atoms have been returned to their bulk positions. Some disorder remains, possibly due to cooling too rapidly.

in the middle of the band gap so that its position is not violated. In effect, the calculation is made legitimate because we only use a small number of recursion levels in the static minimization and we use a square-root terminator for a single band.

4.1.2. The Si(110)-1 × 1 surface. The tilt angle of 31.3° for the relaxed surface we find with LCN (see figures 2(*a*) and (*b*)) is in good agreement with the tilt angle of 30° obtained by Chadi [5]. An untilted surface with a degenerate ground state is not expected according to the Jahn–Teller theorem. Unfortunately, this theorem does not provide any information about the magnitude of the distortion. The breakdown of the surface binding energy given in table 4 allows us to identify the cause of tilting as being largely due to a re-hybridization of the surface atoms and not due to a lowering in the covalent bond energy. Indeed, the breakdown of the individual bond energies given in table 5 shows that despite a strengthening in the two back-bonds to atom 2 as a result of tilting (see the bond energies between atoms 2 and 3 in table 5), the two back-bonds to atom 1 are weakened by a greater amount (see the bond energies between atoms 1 and 2 in table 5). The increase in the covalent bond energy is consistent with the lowering in the

pair potential energy which can only mean that there is a net increase in the average bond length.

4.1.3. Local charge neutrality. The fact that, for the Si(110)–1 × 1 surface, energy minimization without imposing LCN gives rise to a tilt angle of 29.0° and an energy similar to the self-consistent result is significant since it indicates that LCN is unimportant in determining the relaxed atomic configurations of surfaces. The concept of charge transfer and the importance of LCN within the framework of the TBB model has already been discussed in relation to assemblies of atoms in which there is fourfold coordination everywhere (e.g. at grain boundaries) [17]. The result is that in such systems LCN has a negligible effect on the bond forces and hence on the minimized atomic structure. At a surface, however, lower coordination numbers are the rule rather than the exception so the argument needs to be modified accordingly. To clarify the issue here, we note that the Δ_i values will affect the off-diagonal density matrix elements obtained by solving the Hamiltonian. Since the off-diagonal density matrix elements enter into equation (3), it might be expected that removal of the LCN condition would give rise to different relaxed atomic configurations. In contrast, the results indicate that this expectation is not borne out.

We can regard switching off LCN as a perturbation; $\Delta\tilde{\mathbf{H}}$ applied to the self-consistent Hamiltonian $\tilde{\mathbf{H}}^{sc}$ giving a perturbed or non-self-consistent Hamiltonian, $\mathbf{H}^{nsc}$.

$$\mathbf{H}^{nsc} = \mathbf{H}^{sc} + \Delta\mathbf{H}. \tag{14}$$

Here $\Delta\mathbf{H}$ is purely diagonal:

$$\Delta\mathbf{H}_{i\alpha i\beta} = -\Delta_i\delta_{ij}\delta_{\alpha\beta}. \tag{15}$$

Following standard perturbation theory, we can write the surface energy corresponding to the non-self-consistent Hamiltonian E^{nsc} in terms of the surface energy corresponding to the self-consistent Hamiltonian E^{sc} according to

$$E^{nsc} = E^{sc} + E^{(1)} + E^{(2)} + E^{(3)} + \ldots \tag{16}$$

where $E^{(i)}$ is the ith order correction. Within this perturbative scheme we are now asking whether or not $\Delta\mathbf{H}$ is significant.

Note that we define the surface energy E^{surf} to be the binding energy of a semi-infinite system of atoms relative to the binding energy of the same atoms as if they were in the perfect crystal. Explicitly, using equation (1),

$$E^{surf} = Tr(\rho_s^{out} - \rho^f)\mathbf{H}_s + (pp)_s - [Tr(\rho_{pc}^{out} - \rho^f)\mathbf{H}_{pc} + (pp)_{pc}] \tag{17}$$

where the s and pc subscripts refer to the surface and perfect crystal systems respectively, and pp is the pair potential which enters the parametrization. We can regard E^{surf} as a multi-dimensional hypersurface since it is a function of all the atomic positions. The change in the surface energy ΔE^{surf} when the LCN condition is switched off for an assembly of atoms with fixed positions is just

$$\Delta E^{surf} = E^{nsc} - E^{sc}. \tag{18}$$

Using equation (17) we obtain

$$\Delta E^{surf} = Tr(\rho^{nsc} - \rho^f)\mathbf{H}^{nsc} - Tr(\bar{\rho}^{sc}\bar{\rho}^f)\mathbf{H}^{sc}. \tag{19}$$

But $\Delta\mathbf{H}$ is diagonal (equation (15)), so that

$$Tr(\rho^{sc} - \rho^{f})\Delta\mathbf{H} = 0. \tag{20}$$

Combining (19) and (20) it follows that ΔE^{surf} is given *exactly* by

$$\Delta E^{surf} = Tr(\rho^{nsc} - \rho^{sc})\mathbf{H}^{nsc}. \tag{21}$$

Now, since ρ^{nsc} is formed from eigenstates of $\boldsymbol{H}^{nsc}$ it follows that to first order in $\delta\rho^{nsc}$ we have

$$Tr\,\delta\rho^{nsc}\mathbf{H}^{nsc} = 0. \tag{22}$$

As noted by Paxton and Sutton [17], it follows that $E^{(1)}$ is zero. However, the second-order change in the surface energy, $E^{(2)}$, is non-zero. Following Sutton *et al* [20], it may be expressed as

$$E^{(2)} = \int^{E_F} (E - E_F)\Delta N\,dE + \tfrac{1}{2}N(E_F)(\Delta E_F)^2 \tag{23}$$

where ΔN is the change in the total density of states caused by the perturbation $\Delta\mathbf{H}$ and the change in the Fermi energy ΔE_F is given by

$$\Delta E_F = \frac{-1}{N(E_F)}\int^{E_F} \Delta N\,dE. \tag{24}$$

Equation (23) incorporates the condition of global charge conservation. Since, in our model, each atom in the perfect crystal has a finite density of states at the Fermi energy (see figure 1) we argue that $N(E_F)$ is effectively infinite and deduce from equation (24) that ΔE_F is zero. Retaining only the second-order terms in equation (23) we obtain

$$E^{(2)} = \tfrac{1}{2}\sum_{ij}\chi_{ij}\Delta_i\Delta_j \tag{25}$$

where

$$\chi_{ij} = -\frac{\mathrm{Im}}{\pi}\sum_{\alpha\beta}\int^{E_F} G_{i\alpha j\beta}G_{j\beta i\alpha}\,dE. \tag{26}$$

Here we have used the fact that $\Delta\mathbf{H}$ varies linearly with Δ_i. Thus there is no second-order term in $\Delta\mathbf{H}$. By choosing the integration variable to be E/W, where W is the total 'bandwidth', which in our model includes both the valence and condition bands, we obtain

$$\chi_{ij} = -\frac{\mathrm{Im}}{\pi}(1/W)\sum_{\alpha\beta}\int^{E_{F/W}} G_{i\alpha j\beta}(E')G_{j\beta i\alpha}(E')\,dE' \tag{27}$$

where

$$G_{i\alpha j\beta}(E') = \sum_{nk}\langle i\alpha|nk\rangle\langle nk|j\beta\rangle\Big/\left(E' - \frac{E_{nk}}{W}\right). \tag{28}$$

The $|nk\rangle$ label the eigenfunctions of the semi-infinite crystal and the E_{nk} are the corresponding eigenvalues. The Green's functions only have imaginary components for energies that lie within the bands. Consequently, both E' and $E_n\boldsymbol{k}/W$ must be fractional for energies lying within the integration window of equation (27). Assuming that the integrand in (27) is of order unity we deduce that χ_{ij} is of the order E_F/W^2, where E_F is measured from the bottom of the valence band. Thus each term contributing to $E^{(2)}$ in

(25) is of the order $(E_F/2)(\Delta_i W)(\Delta_j/W)$. For $\Delta_i \approx 1$ eV (an upper limit), $E_F \approx 10$ eV and $W \approx 20$ eV we find that each term in (25) is approximately 1/80 eV. This order of magnitude argument explains why the difference in energy of the same surface structure, computed with and without on-site Hamiltonian matrix element shifts of up to 1 eV, is so small. A similar analysis indicates that the change in the force on an atom exerted by a neighbour when the Δ_i values are reset to zero is of the order of $(E_F/W)(\Delta_i/W) \approx 1/40$. Thus each bond force changes at most by a few per cent.

The above discusssion explains why a surface relaxed self-consistently with LCN is likely to fall into the same minimum as a surface relaxed non-self-consistently. The fact that for the Si(110)–1 × 1 surface there are very small differences in the relaxed atomic structures is presumably due to the effect of the above second-order terms in the energy. For the high-energy metastable surface found in the non-self-consistent relaxation of Si(110)–1 × 1 these terms are important enough to the extent that no corresponding minimum could be found when the relaxation was carried out self-consistently. Our results for the Si(110)–1 × 1 surface indicate that if the conformational minimum is a deep well on the energy hypersurface then the second-order terms are not significant despite seemingly very large shifts (~1 eV) in the diagonal Hamiltonian matrix elements required in order to guarantee LCN.

In conclusion, the effect of LCN is to introduce second-order charges in the energy and first-order changes in the interatomic forces. However, since the total bandwidth of the valence and conduction bands is so large compared with typical variations in the on-site Hamiltonian matrix elements, LCN is significant only when energy differences between alternative surface structures are very small, i.e. of the order of a few per cent. It follows that surface reconstructions in general are not driven by charge transfer effects provided the material has a large bandwidth. We note that this study confirms the results of Alerhand and Mele [44] who, by incorporating a Hubbard-like term into their model Hamiltonian, showed that for the Si(100)–2 × 1 surface the on-site repulsion has a relatively minor effect on the magnitude of the tilt angle of the surface dimers.

4.1.4. Energy convergence in the recursion method. The results of the systematic study described in section 2.1.4 and shown in figure 3 show that, although not monotonic, the ISM energy for the ideal and relaxed Si(110)–1 × 1 surface as well as the tilt angle for the relaxed surface do appear to converge as a function of the number of levels. This is important because it means that in working to a small number of levels (e.g. 5–8) we can have confidence in the final structure because we are looking at energy changes which lie outside the noise level of the calculated surface energies, i.e. ±3%. Since we are minimizing the ISM energy functional and not the SDM energy functional we should not be surprised if the final SDM energy is greater than the SDM energy for the ideal surface. Indeed, this is found for the Si(110)–1 × 1 surface when working to five levels and for the Si(111)–2 × 1 surface at seven levels (see table 2).

4.1.5. The Si(100)–2 × 1 surface and localized surface vibrational modes. The Si(100)–2 × 1 surface has been extensively studied by a large number of workers [44–46]. The purpose of this study is to address the question of whether there is any buckling of the surface dimers which are present on this surface.

Low-energy electron diffraction (LEED) experiments appear to be inconclusive with lack of agreement between different groups [47, 48]. STM experiments [49, 50] show that in reality the surface is characterized by a large number of defects, in addition to surface dimers, which may account for this disagreement. It seems that defects are important

for stabilizing this surface: we return to this again briefly in section 4.2. The STM images show the existence of surface dimers with varying degrees of tilt depending on their location relative to defects in the surface. 50% of the dimers appear to be buckled (concentrated near defects) while in the defect-free areas the surface seems to be composed of symmetric unbuckled dimers. In a calculation of the phonon spectrum of the Si(100)–2 × 1 surface, Alerhand and Mele [44] find that there is a localized vibrational mode corresponding to a rocking oscillation of the surface dimers. They also argue that, because a metallic state associated with unbuckled, symmetric dimers has not been observed experimentally, it follows that the surface dimers cannot be symmetric. However, we note that such metallic states have been observed [51, 52] so that symmetric dimers are entirely reasonable.

In our TBB model study we do not attempt to incorporate defects as such a study would be prohibitively expensive in computer time. Thus direct comparison with experiment is not currently possible, although the STM experiments do seem to indicate that the energy difference between the buckled and unbuckled dimer orientations is small. We emphasise that in our *static* calculations we have limited ourselves to a surface periodicity of 2 × 1. Our relaxed configuration consisting of asymmetric buckled dimers (figure 4 and table 6) is essentially the same as that obtained by Chadi [4, 45]. However, we have also shown that a symmetric unbuckled dimer configuration from a relaxation using the Stillinger–Weber potential is equally likely. That a symmetric dimer reconstruction should be stable is contrary to the findings of previous tight-binding studies and agrees with the observations from STM. We note that tilting of the dimers results in a lowering of the promotion energy, as in the case of the Si(110)–1 × 1 surface, as well as a lowering in the covalent bond energy (see table 4). Both these reductions are compensated, however, by an increase of tilting in the pair potential contribution demonstrating that the tilted configuration has net shorter bonds. This is consistent with the large reduction in the bond energy of the two back-bonds to atom 1, as well as the reduction in the covalent bond energy between atoms 1 and 2, which we find on tilting (see table 7). We stress the importance of the reduction in the promotion energy on tilting, for although in this case there is a balance of terms so that neither configuration is preferred, in general this is significant because it shows that there is a strong tendency towards re-hybridization as a means of lowering the surface energy.

During a relaxation when self-consistency was imposed only for every fifth set of computed coordinates (to conserve global charge), we observed the asymmetric buckled dimers flip over to give a buckling in the opposite sense. The effect of not demanding self-consistency for every iteration is to create a discontinuous change in energy as the calculation jumps between energy hypersurfaces. This is equivalent to giving each atom a non-conservative force. The observation strongly suggests that the energy barrier separating the two possible buckling orientations is small. We therefore agree with Alerhand and Mele that a surface vibrational mode may provide a mechanism for interconverting between the various stable and metastable higher order reconstructions such as c(4 × 2) and p(2 × 2) which are found on this surface.

In summary, this theoretical study predicts that both buckled and unbuckled dimer reconstructions should coexist on a defect-free surface. The prediction of symmetric dimers agrees with the observations from STM. Asymmetric dimers, although observed near defects, may also be present in defect-free areas but disguised by means of a surface vibrational mode which results in apparent symmetric dimers as a time-averaged configuration. In confirmation of this, we observe that the energy barrier separating the different energy minima is small.

4.1.6. Π-bonded chain model for the Si(111)–2 × 1 surface. The π-bonded chain model for the Si(111)–2 × 1 surface was originally suggested by Pandey [41–43] and the existence of π-bonded chains has been confirmed by STM measurements [53–56]. Total energy pseudopotential calculations have been performed by Northrup and Cohen [57, 58] who find that a small tilting of the chains in the Pandey model lowers the energy and such buckling has been found experimentally in ion scattering experiments [59, 60]. Dynamical LEED calculations [61, 62], however, find that a small tilt gives a poor fit with experimental LEED data and an improvement is obtained by introducing a much larger tilting of the chains with a vertical difference in position of the two surface atoms parallel to the surface normal (Δz) of 0.38 Å. An independent study [63] came up with similar results ($\Delta z = 0.35$ Å), but in all cases the final fit factor is greater than the maximum value of 0.3 required for confidence. For more details about previous work carried out on this surface the reader is directed to a thorough review article by Pandey [43].

Our results (figure 5 and table 8) predict a tilting of the π-bonded chains ($\Delta z = 0.65$ Å) which is larger than the tilt suggested by LEED, but given the lack of reliability of the LEED fit factor it is reasonable to question the LEED results. It would be interesting to put the structure shown in figure 5(*b*) into a dynamical LEED calculation and thereby achieve a more direct comparison with experiment. The main point is that the TBB model has preserved the basic form of the Pandey model. In addition we can understand what drives the tilting of the π-bonded chains in our results in terms of a reduction in the overall promotion energy (see table 4), which, as for the Si(110)–1 × 1 surface, can be interpreted in terms of a re-hybridization of the surface atoms.

It is pointed out that the STM images are inconclusive regarding the magnitude of the tilt on this surface. Furthermore, it is not clear whether they even confirm the Pandey model since only the top layer is imaged. A new model for this surface proposed by Haneman [46] and based on triple bond cleavage is also consistent with the STM results. Not only does it involve π-bonded chains, but also it explains the STM observation of surface buckling *along* the chains because the atoms in the surface are not in identical environments.

Thus we have confirmed that the TBB model behaves sensibly when relaxing this extensively reconstructed surface and found that tilting of the π-bonded chains is driven by a tendency for the surface atoms to rehybridize. Despite the large experimental effort that has gone into investigating this surface it seems that the detailed atomic structure is still unresolved and that further experiments are necessary.

4.1.7. Rebonding at steps on the Si(113)–1 × 1 surface. High resolution transmission electron microscopy (TEM) experiments have shown [64] that low-energy surfaces need not be confined to high-symmetry orientations and in particular that annealing of a Si(110) thin specimen causes extensive areas of Si(113) to be formed by faceting at the edges of the sample. The periodicity appears to be $n \times 1$ since the TEM image only gives the periodicity along the $[33\bar{2}]$ direction. Salisbury and Huxford [65] conclude that on the basis of present evidence a 1 × 1 rebonding at steps reconstruction is the most probable structure for this surface although more experimental evidence is needed to sort out the periodicity in the $[1\bar{1}0]$ direction. The Si(113) surface has also been investigated by Chadi [6], but his reconstruction is based on the other of the two distinct surfaces with a {113} orientation to that connected with the present study. Very recent LEED experiments [66] indicate that the surface is in fact 3 × 1 reconstructed; we do not consider this reconstruction here.

As summarized in table 2, the relaxed Si(113)–1 × 1 surface has an energy comparable to that of the other surfaces we have studied. The present study has shown that, despite a lowering in the covalent bond energy during relaxation, the major effect is the reduction in the pair potential energy as a result of the highly stretched bonds at the surface (see table 4). While it is encouraging that the Si(113)–1 × 1 surface has a relatively low energy, given the magnitude of the bond distortions, it seems likely that other reconstructions may give a relaxed surface of lower energy. A 3 × 1 reconstructed surface, as suggested by LEED, may well enable some of the distortions present in the 1 × 1 reconstruction to be believed.

4.2. The Stillinger–Weber potential

The SW potential has been used in a large number of simulations including a study of the adatom vibrations on the Si(111)–7 × 7 surface [67, 68] and the melting [69, 70] and equilibrium structure [16, 70, 71] of the Si(100) surface. An evaluation of the SW potential has already been given by Dodson [39] who carried out an MC simulation of epitaxial growth of Si(111). It was found that while the potential worked well for modelling molten Si as well as the bulk properties of Si, modelling the epitaxial growth of Si(111) was impossible due to inadequate treatment of configurations with low coordination numbers. The addition of a fourth-order angular term to the SW potential did not alter the situation. In contrast, molecular-dynamics simulations of epitaxial growth of Si(100) [72] and Si(111) [73] using the SW potential appear to have been more successful. The situation regarding the performance of the SW potential is thus unclear.

Using the results of the TBB model as benchmark calculations, it is the purpose of this section to examine how well the SW potential is able to predict the energy minimized atomic configurations of the four silicon surfaces discussed in section 4.1.

As can be deduced from the form of the SW potential given in section 2.2, the equilibrium condition in diamond cubic silicon is determined only by the pair potential term, because the three-body term is zero when the bond angles all take their ideal tetrahedral values. Since it is only a first-neighbour pair potential, this means that the minimum in the potential occurs at the perfect crystal first neighbour distance. Consequently, all bulk terminated surfaces undergo no relaxation whatsoever in the absence of fluctuations.

Our results show that the buckling predicted by the TBB model, a quantum mechanical phenomenon, cannot be modelled by the classical SW potential which is based solely on geometrical optimisation of bond lengths and angles. The MC simulation strongly suggests, in the case of the Si(111) surface, that the ideal surface is the *global* minimum according to the SW potential (table 11). It is encouraging, however, to note from the MC simulation of the Si(100) surface that defects are incorporated during dimerization since experiment indicates that such defects may well be important in stabilizing this surface.

It is clear that minimization of strain energy for a given number of dangling bonds is the only driving force for lowering the surface energy using this potential. In this context, strain energy is defined as the distortion of, firstly, bond lengths from the ideal value of $\sqrt{\frac{3}{4}}$ LP and secondly, bond angles away from the ideal tetrahedral value of $\cos^{-1}(-\frac{1}{3})$. We have shown that if the reconstruction does not involve a change in the number of bonded neighbours then the SW potential will predict the ideal surface to be the global

minimum. The SW potential cannot reproduce the type of tilting predicted by the TBB model because of the lack of electronic information.

5. Conclusion

By making detailed comparisons with a large number of other experimental and theoretical results we have demonstrated that the TBB model is successfully able to describe the surface structure of a number of silicon surfaces. By examining the various contributions to the surface energy we have been able to provide a clear chemical picture of what drives certain surface reconstructions. This investigation has highlighted the importance of electronic effects, and in particular the promotion energy, in controlling details of the reconstruction such as buckling of the surface atoms. We therefore stress the importance of a quantum mechanical description of interatomic forces for unsaturated bonding environments.

We have provided a detailed discussion of why the assumption of each atom remaining charge neutral, which is a critical assumption in determining an expression for interatomic forces within the framework of the TBB model, in practice makes very little difference to the predicted lowest energy atomic configuration of a surface of silicon. This is significant because it means that in order to obtain a particular atomic structure of a surface of silicon it is not necessary to include charge transfer between atoms on the surface. This conclusion should hold for any material with a total band width comparable to that of silicon (e.g. GaAs).

In our study of the classical potential of Stillinger and Weber we have shown that it does not perform well in predicting stable atomic structures of surfaces due to the lack of electronic information. The results of this and other studies [8] strongly suggest that there is a limit to the empirical parameterisation of configuration space: it is unreasonable to expect a classical potential which has been empirically fitted in one region of configuration space necessarily to perform well in another. One must not, however, lose sight of the aim of classical potentials in terms of their computational efficiency. In order to describe a larger region of configuration space within a single empirical scheme a potential with a greater quantum mechanical basis is required. Thus, an empirical scheme is needed which is a well defined and improveable approximation to the Schrödinger equation. A bond order model recently proposed by Pettifor [18, 19] may go some way towards fulfilling this need.

Acknowledgments

We would like to thank M C Payne for a number of helpful discussions and for providing the Fortran source code which was used to plot out the surfaces shown in the figures. The graphics software was originally written by Y Beppu of Nagoya University, Japan. JHW is thankful to the SERC for providing the necessary funding to carry out this research. JDT has benefited greatly from the backing of Nano Instruments. APS gratefully acknowledges the support of the Royal Society. We thank Professor Sir Peter

Hirsch FRS for providing laboratory facilities. All the calculations were performed on the VAX and CONVEX computers of the Computing Service at Oxford University.

Appendix. Bond forces for the Stillinger–Weber potential

In this appendix we consider the force on an atom arising from the three-body component of the SW potential. It is computationally efficient to express the resultant force on an atom as a sum of 'bond forces' arising from each of its neighbours. By invoking Newton's third law, each bond force contributes to the resultant force on each atom at either end of the bond. Thus, one bond force evaluation contributes to the total force acting on two atoms. This is standard procedure in central pairwise and N-body force models where the bond forces are parallel to the bonds. However, for non-central interactions the division of the resultant force on an atom into a sum of bond forces is more subtle and care has to be taken. We begin by revealing the dangers that exist in this kind of decomposition for the SW three-body potential. We go on to show how these difficulties may be surmounted to arrive at a form for the bond force that obeys Newton's third law.

Consider the three-body component E_3 of the SW potential:

$$E_3 = \sum_{i<j<k} v_3(i, j, k) = \tfrac{1}{6} \sum_{i \neq j \neq k} v_3(i, j, k) \tag{A1}$$

where $v_3(i, j, k)$ is the three-body potential involving atoms i, j and k, given in equations (9), (11) and (12). $v_3(i, j, k)$ is symmetrical with respect to interchanging any of i, j and k and it is translationally invariant. The force in the x direction acting on atom p that arises from all the three-body interactions is $-\partial E_3/\partial x_p$ where x_p is the x coordinate of atom p. This may be expressed as

$$-\frac{\partial E_3}{\partial x_p} = -\left(\sum_{p<j<k} + \sum_{j<p<k} + \sum_{j<k<p} \right) \frac{\partial v_3}{\partial x_p}(p, j, k) \tag{A2}$$

where the sums are taken over j and k only.

We can express the resultant force as a sum of contributions arising from neighbours n. That is, we can re-express (A2) as follows:

$$-\frac{\partial E_3}{\partial x_p} = -\sum_{n \neq p} \left(\frac{\partial E_3}{\partial x_p} \right) \text{due to n}' \tag{A3}$$

where, for $n < p$,

$$\left(\frac{\partial E_3}{\partial x_p} \right)_{\text{due to n}} = \left(\sum_{k>p} + \sum_{n<k<p} + \sum_{k<n} \right) \frac{\partial v_3}{\partial x_p}(p, n, k) \tag{A4}$$

while, for $n > p$,

$$\left(\frac{\partial E_3}{\partial x_p} \right)_{\text{due to n}} = \left(\sum_{k>n} + \sum_{p<k<n} + \sum_{k<p} \right) \frac{\partial v_3}{\partial x_p}(p, n, k). \tag{A5}$$

Care has to be taken with the physical meaning of $-(\partial E_3/\partial x_p)_{\text{due to n}}$. It is tempting to

think of it as the bond force on atom p arising from atom n. However, this interpretation is not consistent with Newton's third law because

$$\left(\frac{\partial E_3}{\partial x_p}\right)_{\text{due to n}} \neq -\left(\frac{\partial E_3}{\partial x_n}\right)_{\text{due to p}}. \tag{A6}$$

Indeed, it may be shown, using the translational invariance of the three-body potential v_3, that for n < p

$$\left(\frac{\partial E_3}{\partial x_p}\right)_{\text{due to n}} + \left(\frac{\partial E_3}{\partial x_n}\right)_{\text{due to p}} = -\left(\sum_{k>p} + \sum_{n<k<p} + \sum_{k<n}\right)\frac{\partial v_3}{\partial x_k}(p, n, k) \tag{A7}$$

and a similar expression may be obtained for n > p. Since the sum in (A.7) is generally non-zero we conclude that $-(\partial E_3/\partial x_p)_{\text{due to n}}$ cannot be interpreted physically as the bond force acting on atom p due to atom n.

We will now demonstrate how the bond force acting on atom p due to atom n may be derived. The crucial step is to separate the components of $v_3(i, j, k)$ that depend on the angles between the three bonds into products of functions that are directed along the bonds. Following Biswas and Hamann [10], this is achieved by using the addition formula of spherical harmonics.

Using (A1), (9) and (11) the three-body energy E_3 may be expressed as follows:

$$E_3 = \frac{\varepsilon}{2}\sum_{i\neq j\neq k} h(r'_{ji}, r'_{jk}, \theta_{ijk}) \tag{A8}$$

where $r' = r/\sigma$ and h is given by (12). The parts of h that depend only on the bond lengths are already separated:

$$h(r'_{ji}, r'_{jk}, \theta_{ijk}) = \xi(r'_{ji})\xi(r'_{jk})g(\cos\theta_{ijk}) \tag{A9}$$

where $\xi(r) = \{\lambda \exp[\gamma(r-a)^{-1}]\}^{1/2}$ and $g(\cos\theta) = (\frac{1}{3} + \cos\theta)^2$. Using the addition formula of spherical harmonics we may write

$$g(\cos\theta_{ijk}) = \sum_{\iota=0}^{2} \frac{4\pi c_\iota}{2\iota+1} \sum_{m=-\iota}^{\iota} Y_{\iota m}(\theta_{ji}, \varphi_{ji}) Y^*_{\iota m}(\theta_{jk}, \varphi_{jk}) \tag{A10}$$

where $c_0 = 4/9$ and $c_1 = c_2 = \frac{2}{3}$. θ_{ji} and φ_{ji} are the spherical polar coordinates directed along the bond vector $\boldsymbol{r}_i - \boldsymbol{r}_j$. The three-body energy may now be reexpressed as follows:

$$E_3 = \frac{\varepsilon}{2}\sum_j \sum_{\iota=0}^{2}\left(\frac{4\pi}{2\iota+1}\sum_{m=-\iota}^{\iota}\Phi^j_{\iota m}\Phi^{j*}_{\iota m} - \sum_{i\neq j}\xi^2(r_{ji})\right) c_\iota \tag{A11}$$

where

$$\Phi^j_{\iota m} = \sum_{i\neq j}\psi_{\iota m}(\boldsymbol{r}_{ji}) \tag{A12}$$

$$\psi_{\iota m}(\boldsymbol{r}_{ji}) = \xi(r_{ji})Y_{\iota m}(\theta_{ji}, \varphi_{ji}). \tag{A13}$$

Then $-\partial E_3/\partial x_p$ may again be expressed in the form of (A3) where the new form of $(\partial E_3/\partial x_p)_{\text{due to n}}$ is as follows:

$$\left(\frac{\partial E_3}{\partial x_p}\right)_{\text{due to n}} = \frac{\varepsilon}{2}\sum_{\iota=0}^{2}\frac{4\pi c\iota}{2\iota+1}\sum_{m=-\iota}^{\iota}\left(\frac{\partial \psi_{\iota m}}{\partial x_m}(\boldsymbol{r}_{np})[\Phi_{\iota m}^{p^*} + (-1)^{\iota}\Phi_{\iota m}^{n^*}] + \text{cc}\right)$$
$$- 2\varepsilon\sum_{\iota=0}^{2} c_\iota \xi(r_{np})\frac{\partial \xi(r_{np})}{\partial x_p}. \tag{A14}$$

It may be verified that

$$\left(\frac{\partial E_3}{\partial x_p}\right)_{\text{due to n}} = -\left(\frac{\partial E_3}{\partial x_n}\right)_{\text{due to p'}} \tag{A15}$$

and thus (A14) does indeed represent the bond force on atom p due to atom n.

References

[1] Hansma P K and Tersoff J 1987 *J. Appl. Phys.* **61** R1
[2] Needels M, Payne M C and Joannopoulos 1987 *Phys. Rev. Lett.* **58** 1765
[3] Chadi D J 1978 *Phys. Rev. Lett.* **41** 1062
[4] Chadi D J 1979 *Phys. Rev. Lett.* **43** 43
[5] Chadi D J 1979 *Phys. Rev.* B **19** 2074
[6] Chadi D J 1984 *Phys. Rev.* B **29** 785
[7] Q Guo-Xin and Chadi D J 1987 *Phys. Rev.* B **35** 1288
[8] Baskes M I, Nelson J S and Wright A F 1989 *Phys. Rev.* B **40** 6085
[9] Khor K E and Das Sarma S 1989 *Phys. Rev.* B **40** 1319
[10] Biswas R and Hamann D R 1985 *Phys. Rev. Lett.* **55** 2001
[11] Stillinger F and Weber T 1985 *Phys. Rev.* B **31** 5262
[12] Tersoff J 1986 *Phys. Rev. Lett.* **56** 632
[13] Tersoff J 1988 *Phys. Rev.* B **37** 6991
[14] Tersoff J 1989 *Phys. Rev.* B **39** 5566
[15] Dodson B W 1987 *Phys. Rev.* B **35** 2795
[16] Khor K E and Das Sarma S 1987 *Phys. Rev.* B **36** 7733
[17] Paxton A T and Sutton A P 1989 *Acta Metall.* **37** 1693
[18] Pettifor D G 1990 *Many-Atom Interactions in Solids (Springer Series in Solid State Sciences vol)* (Berlin: Springer) to be published
[19] Pettifor D G 1989 *Phys. Rev. Lett.* **63** 2480
[20] Sutton A P, Finnis M W, Pettifor D G and Ohta Y 1988 *J. Phys. C: Solid State Phys.* **21** 35
[21] Pettifor D G 1976 *Commun. Phys.* **1** 141
[22] Pettifor D G 1978 *J. Chem. Phys. Lett.* **69** 2930
[23] Mackintosh A R and Andersen O K 1980 *Electrons at the Fermi Surface* ed M Springford (Cambridge: Cambridge University Pres) ch 5.3
[24] Pettifor D G 1987 *Solid State Physics* vol 40 (New York: Academic) p 43
[25] Harris J 1985 *Phys. Rev.* B **31** 1770
[26] Foulkes M 1987 *PhD Thesis* University of Cambridge
[27] Hohenberg P and Kohn W 1964 *Phys. Rev.* **136** B 864
[28] Kohn W and Sham L J 1965 *Phys. Rev.* **140** A 113
[29] Harrison W A 1980 *Electronic Structure and the Properties of Solids* (San Francisco: Freeman)
[30] Slater J C and Koster G F 1954 *Phys. Rev.* **94** 1498
[31] Heine V, Haydock R, Bullett D W and Kelly M J 1980 *Solid State Physics* vol 35 (New York: Academic)
[32] Hashimoto M, Ishida Y, Yamamoto R and Doyama M 1984 *Acta Metall.* **32** 1
[33] Hashimoto M, Ishida Y, Wakayama S, Yamamoto R, Doyama M and Fujiwara T 1984 *Acta Metall.* **32** 13
[34] Nex C M M 1989 *J. Phys. A: Math. Gen.* **11** 653

[35] Glanville S, Paxton A T and Finnis M W 1988 *J. Phys. F: Met. Phys.* **8** 693
[36] Greig D M 1980 *Optimization* (London: Longman) p 56
[37] Paxton A T, Sutton A P and Nex C M M 1987 *J. Phys. C: Solid State Phys.* **20** L263
[38] Inoue J and Ohta Y 1987 *J. Phys. C: Solid State Phys.* **20** 1947
[39] Dodson B W 1986 *Phys. Rev.* B **33** 7361
[40] Allen M P and Tildesley D J 1987 *Computer Simulation of Liquids* (Oxford: Clarendon)
[41] Pandey K C 1981 *Phys. Rev. Lett.* **47** 223
[42] Pandey K C 1981 *Phys. Rev. Lett.* **47** 1913
[43] Pandey K C 1982 *Phys. Rev. Lett.* **49** 223
[44] Alerhand O L and Mele E J 1987 *Phys. Rev.* B **35** 5533
[45] Chadi D J 1979 *J. Vac. Sci. Technol.* **16** 1290
[46] Haneman D 1987 *Rep. Prog. Phys.* **50** 1054
[47] Holland B W, Duke C B and Paton A 1984 *Surf. Sci.* **140** L269
[48] Shu Y S, Yang W S, Jona F and Marcus P M 1985 *The Structure of Surfaces* ed M A Van Hove and S Y Tong (New York: Springer) p 293
[49] Tromp R M, Hamers R J and Demuth J E 1985 *Phys. Rev. Lett.* **55** 1303
[50] Hamers R J, Tromp R M and Demuth J E 1986 *Phys. Rev. Lett.* **56** 1972
[51] Mårtensson P, Cricenti A and Hansson G V 1986 *Phys. Rev.* B **33** 8855
[52] Goldman A, Koke P, Mönch W, Wolfgarten G and Pollmann J 1986 *Surf. Sci.* **169** 438
[53] Feenstra R M, Thompson W A and Fein A P 1986 *Phys. Rev. Lett.* **56** 608
[54] Feenstra R M, Thompson W A and Fein A P 1986 *J. Vac. Sci. Technol.* A **4** 1315
[55] Feenstra R M and Fein A P 1986 *IBM J. Res. Dev.* **30** 466
[56] Stroscio J A, Feenstra R M and Fein A P 1986 *Phys. Rev. Lett.* **57** 2579
[57] Northrup J E and Cohen M L 1983 *Physica* B **117/118** 774
[58] Northrup J E and Cohen M L 1983 *Phys. Rev.* B **27** 6553
[59] Tromp R M, Smeenk R G, Saris F W and Chadi D J 1983 *Surf. Sci.* **133** 137
[60] Tromp R M, Smit L and van der Veen J F 1983 *Phys. Rev. Lett.* **51** 1672
[61] Batra I P, Himsel F J, Marcus P M, Tromp R M, Cook M R, Jona F and Liu H 1985 *The Structure of Surfaces* ed M A Van Hove and S Y Tong (New York:Springer) p 285
[62] Himsel F J, Marcus P M, Tromp R M, Batra I P, Cook M R, Jona F and Liu H 1984 *Phys. Rev.* B **30** 2257
[63] Sakama H, Kawaza A and Ueda K 1986 *Phys. Rev.* B **34** 1367
[64] Gibson J M, McDonald M L and Unterwald F C 1985 *Phys. Rev. Lett.* **55** 1765
[65] Salisbury I G and Huxford N P 1987 *Phil. Mag. Lett.* **56** 35
[66] Yang Y and Williams E D 1989 *36th Nat. Symp. of the American Vacuum Society (1989)*
[67] Li X-P, Allen P B and Broughton J Q 1988 *Phys. Rev. Lett.* **61** 243
[68] Daum W, Ibach H and Müller J E 1988 *Phys. Rev. Lett.* **61** 244
[69] Landman U, Luedtke W D, Barnett R B, Cleveland C L, Ribarsky M W, Arnold E, Ramesh S, Baumgart H, Martinez A and Khan B 1986 *Phys. Rev. Lett.* **56** 155
[70] Lampinen J, Nieminen R M and Kaski K 1988 *Surf. Sci.* **200** 101
[71] Abraham F F and Batra I P 1985 *Surf. Sci.* **163** L752
[72] Lampinen J, Nieminen R M and Kaski K 1988 *Surf. Sci.* **203** 201
[73] Schneider M, Schnuller I K and Rahman A 1987 *Phys. Rev.* B **36** 1340